Solar Energy Materials & Solar Cells 93 (2009) 1417–1422

Contents lists available at ScienceDirect

Solar Energy Materials & Solar Cells

journal homepage: www.elsevier.com/locate/solmat

Synthesis of nanostructured Al-doped zinc oxide films on Si for solar cells applications

O. Lupan [a,b,*], S. Shishiyanu [a], V. Ursaki [c,d], H. Khallaf [b], L. Chow [b], T. Shishiyanu [a], V. Sontea [a], E. Monaico [d], S. Railean [e]

[a] Department of Microelectronics and Semiconductor Devices, Technical University of Moldova, 168 Stefan Cel Mare Blvd., Chisinau, MD 2004, Republic of Moldova
[b] Department of Physics, University of Central Florida, 4000 Central Florida Blvd, Orlando, FL 32816-2385, USA
[c] Laboratory of Low-Dimensional Semiconductor Structures, Institute of Applied Physics, Academy of Sciences of Moldova, 5 Academy Street, Chisinau, MD 2028, Moldova
[d] National Center for Materials Study and Testing, Technical University of Moldova, 168 Stefan Cel Mare Blvd., Chisinau, MD 2004, Republic of Moldova
[e] Institute of Electronic Engineering and Industrial Technologies, Academy of Sciences of Moldova, 5 Academy Street, Chisinau, MD 2028, Moldova

ARTICLE INFO

Article history:
Received 15 March 2008
Received in revised form
8 March 2009
Accepted 14 March 2009
Available online 17 April 2009

Keywords:
Nanostructures
Zinc Oxide
Chemical synthesis
Electrical properties
Photoluminescence

ABSTRACT

Al-doped ZnO thin films have been prepared by a novel successive chemical solution deposition technique. The variation in morphological, structural, electrical, and optical properties of nanostructured films with doping concentration is investigated in details. It was demonstrated that rapid photothermal processing (RPP) improves the quality of nanostructured ZnO films according to the enhancement of resonant Raman scattering efficiency, and the suppression of the visible luminescence with the increase of RPP temperature. It was found from the *I–V* characteristics of ZnO/Si heterojunction that the average short-circuit current density is about 8 mA/cm^2. For 1%Al-doped ZnO/SiO_2/Si structure, the short-circuit current density is about 28 mA/cm^2. The improvement shown in the characteristics may be assigned partially to the reduction of the defect density in the nanostructured Al-doped ZnO films after RPP. The correlations between the composition, microstructure of the films and the properties of the solar cell structures are discussed. The successive chemically deposited Al-doped ZnO thin film offers wider applications of low-cost solar cells in heterojunction structures.

1. Introduction

Solar power as a clean and economical energy source plays an important role in the 21st century in a low greenhouse gas future. Although the sun provides about 12×10^4 TW of solar energy, the whole earth needs to consume about 12–14 TW. Thin film-based solar cells hold greater opportunity to reduce the solar energy cost.

Different types of solar cells have been studied, but among them heterojunction thin film solar cells on single-crystalline Si are preferred due to their high conversion efficiency (>24%). In order to overcome one shortcoming of these cells, high cost, transparent conducting semiconductor/Si heterojunction is investigated. Among the various semiconducting metal oxide materials, the most convenient conducting oxide for solar energy applications is zinc oxide.

The compound semiconductor zinc oxide has a direct bandgap of 3.37 eV (at 300 K), a high melting point of 2248 K, and a large exciton binding energy (60 meV) and wurtzite structure similar to GaN [1]. ZnO is a multifunctional semiconductor material that can be used in many applications such as antireflection coatings, window material for displays, piezoelectric transducers, surface acoustic wave devices, and sensors [1,2]. Zinc oxide can be used as nanostructured electrodes for solar cells [3] because its physical and electrical properties can be controlled by appropriate doping either by cationic (Al, In) or by anionic (F) substitution [4], as well as by deposition parameters and post-growth annealing. Studies on nanostructured semiconducting oxide films for nanotechnology applications [5,6] demonstrated that the photocurrent can be improved by increasing the effective surface area of the ZnO electrode [6–8]. The high conversion efficiency of nanostructured ZnO films based on Al-doped crystallites [8,9] triggered investigations of novel synthesis techniques for fabrication of nanocrystalline ZnO for efficient solar cells. Recently, Al-doped ZnO thin films have attracted attention as a replacement for ITO (tin-doped indium oxide) due to their low resistivity, high transmission, non-toxicity, and low-cost. In addition, zinc oxide production is compatible with current microelectronic technology.

In this context, chemical deposition at low temperatures [2,10–17], and especially the successive chemical solution deposition (SCSD) method [12,15,16] is emerging as a possible alternative to vapor deposition techniques in vacuum or the sol–gel

* Corresponding author at: Department of Microelectronics and Semiconductor Devices, Technical University of Moldova, 168 Stefan Cel Mare Blvd., Chisinau, MD 2004, Republic of Moldova. Tel.: +373 69222260; fax: +373 22497007.
E-mail address: lupan@physics.ucf.edu (O. Lupan).

0927-0248/$ - see front matter © 2009 Elsevier B.V. All rights reserved.
doi:10.1016/j.solmat.2009.03.012

method. SCSD is a simple, scalable, flexible, and inexpensive method to grow thin films. It offers an easy way to dope film through a well-controlled heterogeneous reaction. This method does not require high-quality substrates, can operate at room temperature, and does not need vacuum. The growth parameters are relatively easy to control and the stoichiometric synthesis can be obtained [15–18]. Although many papers have been reported on ZnO films, the SCSD synthesis and post-grown rapid photothermal processing (RPP) of nanostructured Al-doped ZnO have not been extensively studied for solar cell applications. These techniques can contribute substantially to cost-effective solar cells production in the future.

This paper reports the SCSD method to deposit adherent and uniform nanocrystalline ZnO films. The effects of Al dopant concentration as well as the effect of RPP temperature on structure, morphology and photoluminescence (PL) characteristics of deposited ZnO films are investigated.

2. Experimental

The used aqueous zinc complex solution comprises a mixture of zinc sulfate ($Zn(SO_4)\cdot 7H_2O$), aluminum sulfate ($Al_2(SO_4)_3\cdot 18H_2O$), and sodium hydroxide (NaOH) mixed until complete dissolution. The concentration of the complex solution was diluted to obtain 0.05–0.15 M zinc concentration for deposition by adding respective quantities of deionized (DI) water according to the results of previous investigations [12,13,20]. The pH value of the solution was about 10.5 in these experiments. Aluminum-doped zinc oxide films were deposited on Si substrates by a very simple SCSD method. A standard procedure described in Refs. [19,20] was used to clean the silicon substrate surfaces, prior to the cell preparation.

The SCSD synthesis of aluminum-doped zinc oxide films can be found in our previous work [2,12]. The Al doping of ZnO films was achieved by adding $Al_2(SO_4)_3\cdot 18H_2O$ in the aqueous solution corresponding to 0.5, 1, 2, 3 or 6 at% Al. The complex solution of cations (bath #1) and DI water (baths #2 and #4) for intermediate rinsing was kept at room temperature and the beaker with DI water as anionic precursor (bath #3) was kept at 95–98 °C during deposition.

The successive chemical solution deposition is based on the adsorption and reaction of zinc complex ions from the aqueous complex solution kept at room temperature and immersion of the wet substrate in the anionic solution. Rinsing with water is performed between the successive immersions. During SCSD of nanostructured ZnO thin films, we followed four steps for a full growth cycle, which are described in details elsewhere [2,12]. The duration of each step in the solution was maintained at 3 s. The deposition cycles were repeated until a desired thickness was reached according to the previously studied growth kinetics [13,20]. High-quality thin films with a resistivity of about $1\times10^{-3}\,\Omega\,cm$ were synthesized by increasing the duration of the immersion procedure described above to 5 s in the first and third steps, and to more than 10 s in the second and fourth steps. The goal of the present work is to grow and study nanostructured adherent Al–ZnO films on Si and SiO_2/Si substrates. Synthesized films have undergone rapid photothermal processing (RPP) at temperatures between 200 and 800 °C in vacuum using an IFO-6 RPP system [13,19]. The duration and temperature of post-growth RPP processing applied to films were 20 s and 650 °C,respectively according to the previous work [2,20].

The surface morphology of films with different aluminum-doping concentrations was examined using a VEGA TS 5130MM scanning electron microscope equipped with an energy dispersion X-ray spectrometer (EDX). Crystalline characteristics of deposited films were studied by X-ray diffraction (XRD) with a Rigaku diffractometer using Cu-K_α radiation ($\lambda = 1.54178$ Å) and optimized operating conditions of 30 mA and 40 kV. The diffraction angle 2θ was scanned from 10° to 90° at the scanning speed of 0.04° per second. The composition measurements of ZnO films were performed by Rutherford back scattering (RBS) General IONEX 1.7 MV Tandetron and EDX.

The photoluminescence of ZnO films was excited by the 351.1 nm line of an Ar^+ Spectra Physics laser and analyzed in a quasi-backscattering geometry through a double spectrometer with 1200 grooves/mm gratings, assuring a linear dispersion of 0.8 nm/mm. This corresponds to a spectral resolution of 0.5 meV. The laser beam was transmitted through variable attenuators. The samples were mounted on the cold station of an LTS-22-C-330 optical cryogenic system and all measurements were performed at 10 K.

Ohmic contacts were fabricated with Al metal deposited onto the surface of ZnO films and at the rear surface of Si substrate in a vacuum system. Electrical characterization was performed using the two-point probe method in the temperature range 300–600 K. The n-type conductivity exhibited by zinc oxide films was confirmed using an Ecopia Hall effect measurement system. *I–V* characteristics were performed at room temperature using Measure Unit of semiconductor devices characteristics "L2-56" under a simulated AM1.5 solar spectrum 100 mW/cm^2 (PRM 500 W Xenon lamp, model number 20101 as light source).

3. Results and discussions

Fig. 1 shows the effect of Al doping on the morphologies of nanostructured ZnO films on silicon substrate. The morphology of pure ZnO films is presented in Fig. 1(a). The increase in Al concentration up to 1.0 at% reduces the average nanoparticle dimension to about 100 nm (see Fig. 1(b)) and increases the aspect ratio in comparison to pure ZnO films (0.0 at% Al). The increase in Al doping from 1 to 6 at% leads to the increase of particle size (Figs. 1c and d). Fig. 1(c) shows the SEM image of 4 at% Al-doped ZnO films after RPP at 650 °C, 20 s (sample 1.4P). Fig. 1(d) presents the morphology of the 6 at% Al-doped ZnO film (sample 1.6). The increase in doping with Al of ZnO films from 4% (sample 1.4P) to 6% (sample 1.6) not only leads to the increase of particle size (Figs. 1(c) and (d)) but also leads to the change in film structure. This behavior can be explained in terms of segregation of Al content into the grain boundaries. At the same time, the independence of surface morphology of RPP temperature up to 650 °C was observed from SEM for pure and Al-doped films.

According to our experimental results, the most important conditions of synthesis that contribute to the variations of Al-doped ZnO films' morphology are related to the duration of substrate immersions (from 1 to 30 s) and the number of successive dipping steps (from 1 to 4) in aqueous solution baths.

The XRD spectra of as-grown pure ZnO films, ZnO-doped with 1.0 and 2.0 at% Al, are presented in Fig. 2 by curves (a), (c), and (e). The influence of RPP on the XRD pattern is also studied and presented by curves (b) and (d) in Fig. 2. The peaks of hexagonal wurtzite-type ZnO [space group: $P6_3mc(186)$; $a = 0.3249$ nm, $c = 0.5206$ nm] structure are present. All diffraction results are in agreement with the JCPDS 036-1451 card for ZnO [21]. The intensity of peaks relative to the background signal demonstrates a high crystalline quality of the ZnO hexagonal phase of the products grown by SCSD and RPP. From Fig. 2, the increase in the intensity of XRD signals in the investigated samples can be observed. Through the variation of the duration of maintenance in aqueous solutions during the four-step SCSD process, one can improve the crystallinity and tune the physical properties of the

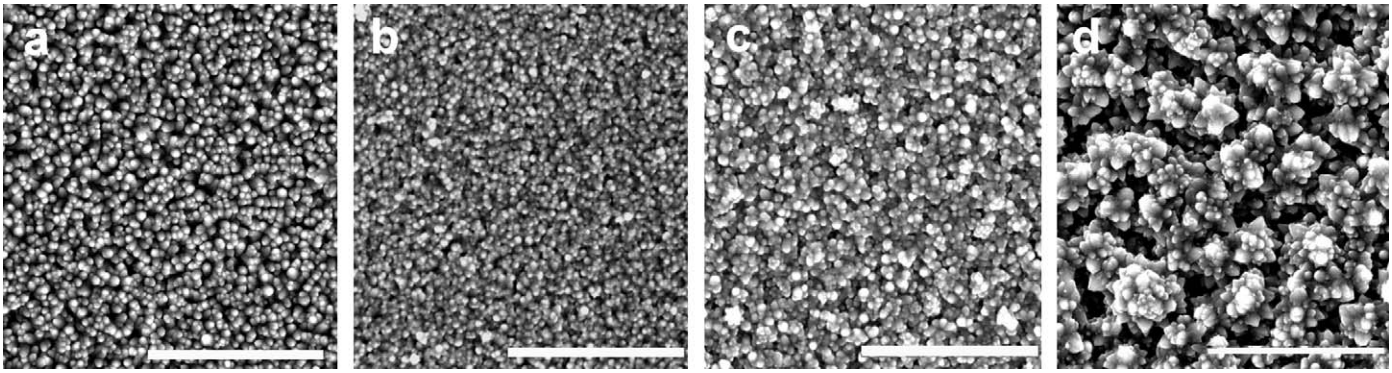

Fig. 1. Secondary electron micrographs of undoped and doped ZnO films onto glass substrates showing the influence of doping and RPP annealing on surface morphology: (a) undoped as-grown film (sample 1.0), (b) as-grown 1 at% Al-doped ZnO (sample 1.1), (c) 4 at% Al-doped ZnO after the RPP 650 °C, 20 s (sample 1.4P), and (d) 6 at% Al-doped ZnO (sample 1.6). The scale bar is 10 μm.

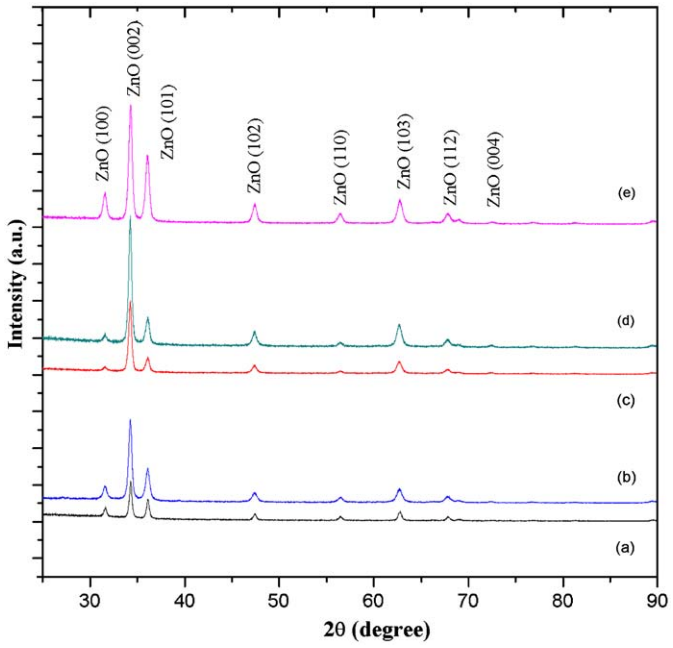

Fig. 2. The XRD pattern of ZnO films with Al doping concentration of (a) as-grown pure ZnO films, (b) pure ZnO films after RPP at 650 °C, (c) 1 at% Al ZnO films as-grown, (d) 1 at% Al ZnO films after RPP at 650 °C, and (e) 2 at% Al ZnO films after RPP at 650 °C.

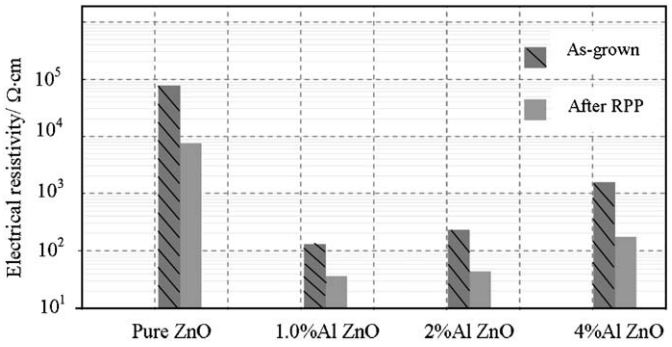

Fig. 3. Electrical resistivity values versus dopant concentration of different as-grown and subjected to RPP (650 °C for 20 s) ZnO films.

films. In our experiments, we observed a de-orientation of crystal growth from the (0 0 2) direction with the increase of Al-doping concentration from 1.0 to 2.0 at%. The mean crystallite grain size of nanostructured ZnO samples was calculated using Scherrer's formula [22]. This mean grain size determined from the XRD line broadening is 240 and 224 Å for undoped ZnO (sample 1.0) and Al-doped ZnO films (sample 1.1), respectively. The crystallite sizes were nearly the same for ZnO films before and after RPP, which is in agreement with previous results of Al-doped ZnO [23].

The lattice parameters have been calculated using the relation [24]

$$\frac{1}{d_{hkl}^2} = \frac{4}{3}\left(\frac{h^2+hk+k^2}{a^2}\right) + \frac{l^2}{c^2}$$

The d_{hkl} parameter was deduced from the XRD pattern. The mean values are $a = 3.253$ A and $c = 5.209$ A, which are in accordance with the previously reported results [23,24].

The Al/Zn ratios in films were analyzed by RBS and EDX measurement and a linear correlation was found in the investigated range of 1–6 at%. The Al/Zn ratios surveyed are 1/99 and 4/96 (at%) in different scanned regions on investigated samples (samples 1.1 and 1.4).

The pure ZnO films have lower stability in corrosive, humid ambient due to the large amount of oxygen (O) vacancy [25]. The properties of such zinc oxide films are often altered by adsorption of O_2 and water. Another factor limiting the application of pure ZnO as a transparent conductive film in solar cells is its thermal instability. To overcome these disadvantages, ZnO films are controlled by appropriate doping either by cationic (Al, In) or by anionic (F) substitution [4] and post-growth annealing. It has been documented [4] that the variation range of resistivity is about 5% for temperature increase from 50 to 400 °C in air when the content of Al in ZnO is 0.5–1.0 at%. The doping with Al in ZnO showed conductivity enhancement along with improved transparency [26,27] and mechanical stability [4]. Therefore, SCSD-grown ZnO films have been doped with Al to improve their properties and electrical characteristics.

Fig. 3 shows the electrical resistivity of the undoped and Al-doped ZnO thin films versus dopant concentration and RPP annealing at 650 °C for 20 s. The electrical resistivity decreases with Al doping as well as with rapid photothermal processing at 650 °C. For example, in our experiments pure ZnO films showed electrical resistivity of about $10^5\,\Omega$ cm and 1% Al-doped ZnO showed $10^2\,\Omega$ cm, which was decreased by RPP at 650 °C for 20 s (Fig. 3).

The decrease in resistivity with Al doping is due to the fact that Al going into Zn site will have one extra electron. This indicates that an effective substitution results in a higher amount of

generated conduction electrons. This could be a reason for the decrease in film resistivity. The resistivity of Al-doped ZnO films is found to decrease with aluminum concentration up to 2 at%. This can be explained by the fact that the ionic radius of aluminum is smaller than that of Zn. So the decrease in resistivity with dopant concentration is also due to the replacement of Zn^{2+} by Al^{3+} ions. Irreversible changes in electrical characteristics have been observed when the ZnO films were subjected to post-growth rapid photothermal processing at temperatures higher than 300 °C for 20 s duration. In the temperature range of 550–650 °C, improvement in the stability of ZnO samples has been observed. According to our experimental measurements the Al-doped ZnO-based samples have higher conductance stability in comparison to pure ZnO films.

The ZnO films doped with 1.0 at% Al showed n-type conductivity after RPP and electrical resistivity of about 40 Ω cm. These films can be used as nanostructured electrode in heterojunction solar cells.

Fig. 4 shows the photoluminescence spectra of an undoped ZnO film before (curve 1—sample 1.0) and after RPP at 650 °C (curve 2—sample 1.0P). The PL of the undoped ZnO films is dominated by red, yellow, and green emissions (see Fig. 4) usually associated with Zn_i, O_i, and V_o structural defects, respectively [28–30], while the emission spectrum in the near-bandgap emission is dominated by multiphonon resonant Raman scattering. The RPP of the as-grown film leads to a decrease in the defect-related PL by a factor of ten, therefore indicating a decrease in the defect concentration. One can conclude that RPP, apart from improving the crystal quality deduced from the XRD, also improves the optical quality of the material. Fig. 5 compares the PL spectra of ZnO films doped with different concentrations of Al (samples 1.05P, 1.1P, and 1.3P). One can see from Fig. 5 that Al doping leads to a decrease in both the red and green luminescence, the decrease in the green emission being more pronounced. It was also previously observed that introducing Al into ZnO thin films results in the depression of the PL from oxygen or Zn defects [31]. In contrast to the undoped films, the Al-doped films exhibit in the near-bandgap spectral range a broad PL band in addition to the multiphonon resonant Raman scattering signal (see the inset in Fig. 5). The full-width at half-maximum (FWHM) of this PL band increases considerably with increase in Al concentration. For instance, FWHM increases from 80 to 150 meV with the increase in Al concentration from 0.5 to 3.0 at%. A detailed investigation of the nature of this near-bandgap PL band carried out elsewhere [32,33] demonstrated that it is mainly due to direct transitions of electrons between the conduction and valence band tails. The broadening of the PL band involved can be accounted for by the broadening of the band edges due to potential fluctuations induced by the high concentration of Al impurity. The width of the band tails and the dependence of the FWHM of the PL band on carrier concentration can be calculated using the model for broadening of impurity bands in heavily doped semiconductors developed by Morgan [34]. One can estimate from the analysis of the FWHM of the PL band [20,32,33] that the free carrier concentration increases from 7.0×10^{19} to $2.5\times10^{20}\,cm^{-3}$ with the increase in Al concentration from 0.5 to 3.0 at%.

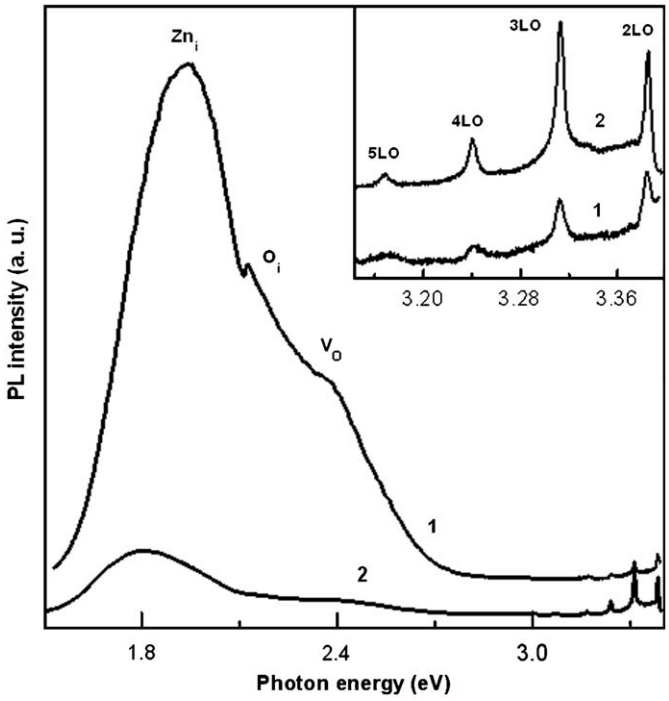

Fig. 4. Photoluminescence spectra of undoped ZnO film before (curve 1—sample 1.0) and after RPP at 650 °C (curve 2—sample 1.0P). Inset is the near-bandgap emission spectrum of films 1.0 (curve 1) and 1.0P (curve 2).

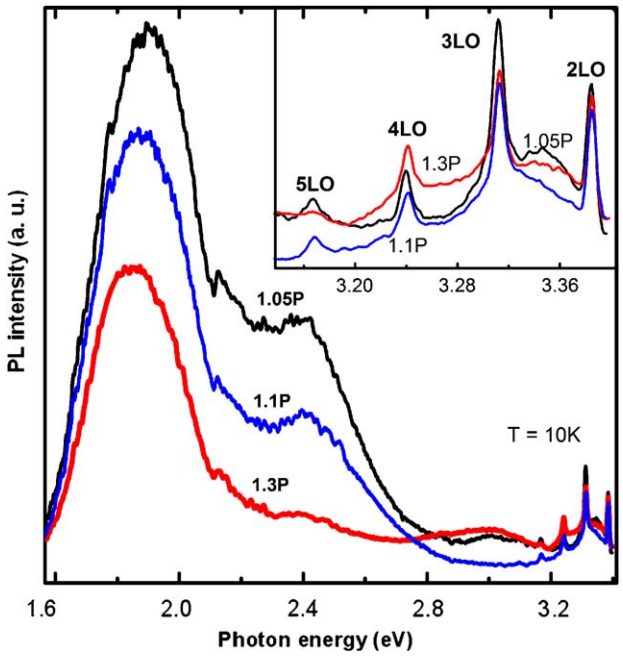

Fig. 5. Photoluminescence spectra of ZnO films with different Al doping concentrations subjected to RPP at 650 °C as presented (0.5, 1.0, and 3.0 at% Al as sample 1.05P, 1.1P, and 1.3P, respectively). Inset is the near-bandgap emission spectrum of films 1.05P, 1.1P, and 1.3P.

Next we investigated the possibility of using these films as nanostructured electrode in heterojunction solar cells. Among different cost-effective solar cell structures, the nanostructured transparent conducting oxide–semiconductor heterojunction attracted attention due to its simple structure and relative high conversion efficiencies. Also, silicon is one of the cheapest wafer materials with a cubic structure [35].

Cells with an area of 0.9 cm^2 were fabricated on Si substrate of 6 cm^2. The cells were prepared in one run, so the preparation conditions were the same for the as-grown and RPP samples. All cells on ZnO/Si/Al structure have a fill factor of over 0.436. By using RPP, the distribution of the fill factor was improved, which is important for the fabrication of solar cells with larger areas.

Fig. 6 presents the current–voltage (I–V) characteristics of a nanostructured Al–ZnO/Si/Al and Al–ZnO/SiO_2/Si/Al-based solar

cell fabricated by the SCSD method and thermal evaporation of Al back contact. *I–V* characteristics were performed at room temperature using a Measure Unit "L2-56" under simulated AM1.5 solar spectrum as described above. From the investigated *I–V* characteristics of the ZnO/Si heterojunction (Fig. 6, curve 1), it was observed that the average short-circuit current density is about 8 mA/cm^2 for a typical n-ZnO/p-Si heterojunction. It is observed from Fig. 6 (curves 2–5) that the short-circuit current density increases after the RPP of Al–ZnO, which may eliminate the interface states between ZnO and Si. We observed that short-circuit current of ZnO/Si solar cells depends on the interface between ZnO and substrate. For this purpose, rapid photothermal oxidation-grown 10-nm-thin SiO_2 layer was inserted at the interface. The thickness and refractive index of the rapid photothermal oxidation-grown SiO_2 layer were determined by ellipsometry [19]. The refractive index of SiO_2 oxide is about 1.46 and the error of uniformity is in the range 1′–2′. Apart from the reduction of interface states [36], the insertion of SiO_2 layer between ZnO and Si reduces the effect of lattice mismatch and allows a more efficient exploitation of the potential of heterojunction solar cell design [37]. The short-circuit current was increased by inserting an SiO_2 layer between ZnO and Si.

The best stabilized conversion efficiency of 6.8% ($V_{OC} = 0.335$ V; $J_{SC} = 28$ mA/cm^2; FF = 0.721) was achieved for the cell with an area of 1 cm^2 without any antireflection coatings (Fig. 6, curve 5).

It was found that all ZnO/Si heterojunction devices fabricated using ZnO films deposited by the SCSD method exhibit enhanced rectifying current–voltage characteristics after RPP at 600–700 °C. The variation found in the *I–V* characteristics can be caused by the changes in the electrical properties of the n-ZnO layer as well as in the interface region between ZnO/Si layers. These results of improvement shown in rectifying characteristic may be assigned partially to the reduction of the defect density in films after RPP. Also, by the insertion of SiO_2 insulator layer in this structure, a potential barrier for charge carriers will be formed. It is known that the work function of ZnO (4.35 eV) is higher than the electron affinity of silicon (3.5 eV). At zero bias the energy bands of silicon at the SiO_2/Si interface bend upward, but they can be further bent by the presence of insulator charge and/or interface states, and the carrier densities at the interface change. The photo-carrier transport from silicon to ZnO layer through the barrier is considered to be dominated by the quantum mechanical tunneling process of the minority carrier, similar to metal–insulator semiconductor-type solar cells [38]. In this way, the SiO_2 layer creates a potential barrier that will suppress the dark saturation current of the solar cells structure, contributed by the majority carrier, and the photo-voltage of the cells increases [39]. To verify the above hypothesis, a novel type of solar cell was fabricated on a heavily doped silicon (Si^{++}) and labeled as 1%Al-doped ZnO/SiO_2/Si^{++} solar cells (curve 5 in Fig. 6). It demonstrates a higher output photo-voltage compared to the ZnO/Si cell (curve 1 in Fig. 6).

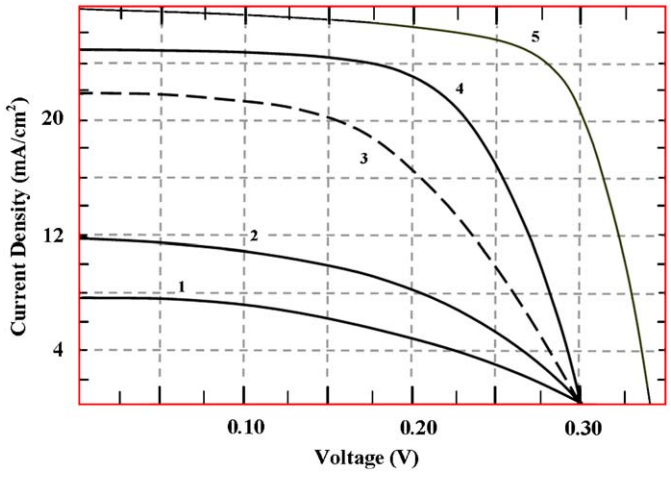

Fig. 6. Current–voltage characteristics of ZnO/Si–based solar cells with pure ZnO after RPP (curve 1); RPP 1 at%Al-doped ZnO/Si (curve 2); as-grown 1 at%Al-doped ZnO/SiO_2/Si (curve 3), and RPP 1%Al-doped ZnO/SiO_2/Si solar cells (curve 4), and RPP 1%Al-doped ZnO/SiO_2/Si^{++} solar cells (curve 5). Illumination was performed with an AM1.5 solar simulator. The characteristics of the element were measured at an illumination intensity of $I_{ill} = 100$ mW/cm^2.

4. Conclusion

Nanostructured ZnO and ZnO:Al thin films were synthesized by a novel successive chemical solution deposition SCSD and rapid photothermal processing RPP. The advantages of this new technology are related to the simplicity of the process, short duration, energy saving, accessible auxiliary materials, non-sophisticated equipment, and structures with high efficiency.

It was found that all ZnO/Si heterojunction devices fabricated using ZnO films deposited by the SCSD method exhibit enhanced rectifying current–voltage characteristics after RPP at 600–700 °C. The variation found in the *I–V* characteristics can be caused by the changes in the electrical properties of n-ZnO layer as well as interface region between the nanostructured film and Si substrate. The improvement shown in rectifying characteristic may be assigned partially to the reduction of the defect density in the films after RPP.

According to the developed technique we fabricated a solar cell with a conversion efficiency of 6.8% ($V_{OC} = 0.335$ V; $J_{SC} = 28$ mA/cm^2; FF = 0.721) for Al–ZnO/SiO_2/Si/Al. The area of the fabricated cell was about 1 cm^2 and no antireflection coatings were employed.

Acknowledgements

This work was made possible in part by Award no. MTFP-1014 B Follow-on of the Moldovan Research and Development Association (MRDA) under funding from the US Civilian Research & Development Foundation (CRDF). Financial support from the Ministry of Education and Science of Moldova (Project 321 b/s) and from Project 025P from the Supreme Council for Research and Technological Development of the ASM are also acknowledged. The research described here was made possible in part by an award of US Department of Agriculture #58-3148-8-175.

References

[1] Ü. Özgür, Ya.I. Alivov, C. Liu, A. Teke, M.A. Reshchikov, S. Dogan, V. Avrutin, S.J. Cho, H.A. Morkoç, A comprehensive review of ZnO materials and devices, J. Appl. Phys. 98 (2005) 041301.
[2] O.I. Lupan, S. Shishiyanu, L. Chow, T. Shishiyanu, Nanostructured zinc oxide gas sensors by successive ionic layer adsorption and reaction method and rapid photothermal processing, Thin Solid Films 516 (2008) 3338–3345.
[3] A.A. Ibrahim, A. Ashour, ZnO/Si solar cell fabricated by spray pyrolysis technique, J. Mater. Sci.: Mater. Electron. 17 (2006) 835–839;
[b] W.W. Wenas, S. Riyadi, Carrier transport in high-efficiency ZnO/SiO_2/Si solar cells, Sol. Energy Mater. Sol. Cells 90 (2006) 3261–3267.
[4] A.V. Singh, R.M. Mehra, A. Yoshida, A. Wakahara, Doping mechanism in aluminum doped zinc oxide films, J. Appl. Phys. 95 (2004) 3640.
[5] V.P. Tolstoy, Successive ionic layer deposition. The use in nanotechnology, Russ. Chem. Rev. 75 (2) (2006) 161–175.
[6] H. Rensmo, K. Keis, H. Lindstrom, S. Sodergren, A. Solbrand, A. Hagfeldt, S.-E. Lindquist, L.N. Wang, M. Muhammed, High light-to-energy conversion efficiencies for solar cells based on nanostructured ZnO electrodes, J. Phys. Chem. B 101 (1997) 2598–2601.
[7] M. Afzaal, P. O'Brien, Recent developments in II–VI and III–VI semiconductors and their applications in solar cells, J. Mater. Chem. 16 (2006) 1597–1602.

[8] M. Matsumura, S. Matsudaira, H. Tsubomura, Dye sensitization and surface structures of semiconductor electrodes, Ind. Eng. Chem. Prod. Res. Dev. 19 (1980) 415–421.
[9] P. Suri, M. Panwar, R.M. Mehra, Photovoltaic performance of dye-sensitized ZnO solar cell based on eosin-Y photosensitizer, Mater. Sci.—Poland 25 (1) (2007) 137–144.
[10] P. Mitra, A.P. Chatterjee, H.S. Maiti, Chemical deposition of ZnO films for gas sensors, J. Mater. Sci.: Mater. Electron. 9 (1998) 441–445.
[11] S. Lindroos, M. Leskela, Growth of zinc peroxide (ZnO_2) and zinc oxide (ZnO) thin films by the successive ionic layer adsorption and reaction–SILAR–technique, Int. J. Inorg. Mater. 2 (2000) 197–201.
[12] O. Lupan, L. Chow, S. Shishiyanu, E. Monaico, T. Shishiyanu, V. Şontea, B. Roldan Cuenya, A. Naitabdi, S. Park, A. Schulte, Nanostructured zinc oxide films synthesized by successive chemical solution deposition for gas sensor applications, Mater. Res. Bull. 44 (2009) 63–69.
[13] S.T. Shishiyanu, T.S. Shishiyanu, O.I. Lupan, Sensing characteristics of tin-doped ZnO thin films as NO_2 gas sensor, Sensors Actuators B 107 (2005) 379–386.
[14] A.E. Rakshani, Thin ZnO films prepared by chemical solution deposition on glass and flexible conducting substrate, Appl. Phys. A 81 (2005) 1497–1502.
[15] A.E. Rakshani, J. Kokaj, J. Mathew, B. Peradeep, Successive chemical solution deposition of ZnO films on flexible steel substrate: structure, photoluminescence and optical transitions, Appl. Phys. A 86 (2007) 377–383.
[16] M. Muhammed, Th. Tsakalakos, Nanostructured materials and nanotechnology: overview, J. Korean Ceram. Soc. 40 (11) (2003) 1027–1046.
[17] Th.P. Niesen, M.R. De Guire, Review: deposition of ceramic thin films at low temperatures from aqueous solutions, J. Electroceram. 6 (3) (2001) 169–207.
[18] H. Nanto, S. Tsubakino, T. Kawai, M. Ikeda, S. Kitagawa, M. Habara, Zinc oxide thin-film chemical sensors in conjunction with neural network pattern recognition for trimethylamine and dimethylamine gases, J. Mater. Sci. 29 (1994) 6529–6532.
[19] S.T. Shishiyanu, O.I. Lupan, T.S. Shishiyanu, V.P. Şontea, S.K. Railean, Properties of SiO_2 thin films prepared by anodic oxidation under UV illumination and rapid photothermal processing, Electrochim. Acta 49 (25) (2004) 4433–4438.
[20] [a] S.T. Shishiyanu, O.I. Lupan, E. Monaico, V.V. Ursaki, T.S. Shishiyanu, I.M. Tiginyanu, Photoluminescence of chemical bath deposited ZnO:Al films treated by rapid thermal annealing, Thin Solid Films 488 (2005) 15–19
[b] O. Lupan, in: Proceedings of the 3rd International Conference on Microelectronics and Computer Science, Moldova, vol. 1, 2002, p. 149–152.
[21] Joint Committee on Powder Diffraction Standards, Powder Diffraction File no. 36-1451.
[22] B.D. Cullity, Elements of X-ray Diffractions, Addison-Wesley, Reading, MA, 1978, p. 102.
[23] S.-Sh. Lin, J.-L. Huang, P. Sajgalik, The properties of heavily Al-doped ZnO films before and after annealing in the different atmosphere, Surf. Coat. Technol. 185 (2004) 254–263.
[24] A. Drici, G. Djeteli, G. Tchangbedji, H. Derouiche, K. Jondo, K. Napo, J.C. Bernède, S. Ouro-Djobo, M. Gbagba, Structured ZnO thin films grown by chemical bath deposition for photovoltaic applications, Phys. Status Solidi (a) 201 (7) (2004) 1528–1536.
[25] D.J. Qiu, H.Z. Wu, A.M. Feng, Y.F. Lao, N.B. Chen, T.N. Xu, Annealing effects on the microstructure and photoluminescence properties of Ni-doped ZnO films, Appl. Surf. Sci. 222 (2004) 263–268.
[26] Z.L. Pei, C. Sun, M.H. Tan, J.Q. Xiao, D.H. Guan, R.F. Huang, L.S. Wen, Optical and electrical properties of direct-current magnetron sputtered ZnO:Al films, J. Appl. Phys. 90 (2001) 3432.
[27] K. Postava, H. Sueki, M. Aoyama, T. Yamaguchi, K. Murakami, Y. Igasaki, Doping effects on optical properties of epitaxial ZnO layers determined by spectroscopic ellipsometry, Appl. Surf. Sci. 175/176 (2001) 543–548.
[28] K. Vanheusden, W.L. Warren, C.H. Seager, D.R. Tallant, J.A. Voigt, Mechanisms behind green photoluminescence in ZnO phosphor powders, J. Appl. Phys. 79 (1996) 7983.
[29] X.L. Wu, G.G. Siu, C.L. Fu, H.C. Ong, Photoluminescence and cathodoluminescence studies of stoichiometric and oxygen-deficient ZnO films, Appl. Phys. Lett. 78 (2001) 2285.
[30] S. Yamauchi, Y. Goto, T. Hariu, Photoluminescence studies of undoped and nitrogen-doped ZnO layers grown by plasma-assisted epitaxy, J. Cryst. Growth 260 (2004) 1–6.
[31] K.-K. Kim, H. Tampo, J.O. Song, T.-Y. Seong, S.-J. Park, J.-M. Lee, S.-W. Kim, S. Fujita, S. Niki, Effect of rapid thermal annealing on Al doped n-ZnO films grown by RF-magnetron sputtering, Jpn. J. Appl. Phys. 44 (2005) 4776–4779.
[32] V.V. Zalamai, V.V. Ursaki, E. Rusu, P. Arabadji, I.M. Tiginyanu, L. Sirbu, Photoluminescence and resonant Raman scattering in highly conductive ZnO layers, Appl. Phys. Lett. 84 (2004) 5168.
[33] V.V. Ursaki, I.M. Tiginyanu, V.V. Zalamai, E.V. Rusu, G.A. Emelchenko, V.M. Masalov, E.N. Samarov, Multiphonon resonant Raman scattering in ZnO crystals and nanostructured layers, Phys. Rev. B 70 (2004) 155204.
[34] T.N. Morgan, Broadening of impurity bands in heavily doped semiconductors, Phys. Rev. 139 (1965) A343.
[35] A. Goetzberger, V.U. Hoffmann, Silicon solar cell material and technology, in: Photovoltaic Solar Energy Generation, vol. 112, Springer, Berlin, Heidelberg, 2005, pp. 23–41.
[36] H. Kobayashi, T. Ishida, Y. Nakato, H. Mori, Mechanism of carrier transport through a silicon-oxide layer for <indium-tin-oxide/silicon-oxide/silicon> solar cells, J. Appl. Phys. 78 (1995) 3931.
[37] R. Klenk, Characterisation and modelling of chalcopyrite solar cells, Thin Solid Films 387 (2001) 135–140.
[38] J. Shewchun, R. Singh, M.A. Green, Theory of metal–insulator–semiconductor solar cells, J. Appl. Phys. 48 (2) (1977) 765.
[39] T. Okuno, Y. Osaka, M. Hirose, Characterization of Si MIS solar cell, Electron. Commun. Jpn. P.I: Commun. 66 (8) (1983) 109.